AIAA 96-0316

Aerothermodynamic Analysis of Commercial Experiment Transporter (COMET) Reentry Capsule

William A. Wood,
Peter A. Gnoffo and
Didier F. G. Rault
NASA Langley Research Center
Hampton, Virginia

34th Aerospace Sciences Meeting & Exhibit
January 15-18, 1996 / Reno, NV

For permission to copy or republish, contact the American Institute of Aeronautics and Astronautics
370 L'Enfant Promenade, S.W., Washington, D.C. 20024

Aerothermodynamic Analysis of Commercial Experiment Transporter (COMET) Reentry Capsule

William A. Wood,* Peter A. Gnoffo† and Didier F. G. Rault‡
NASA Langley Research Center, Hampton, VA 23681

An aerothermodynamic analysis of the Commercial Experiment Transporter (COMET) reentry capsule has been performed using the laminar thin-layer Navier-Stokes solver Langley Aerothermodynamic Upwind Relaxation Algorithm. Flowfield solutions were obtained at Mach numbers 1.5, 2, 5, 10, 15, 20, 25, and 27.5. Axisymmetric and 5, 10, and 20 degree angles of attack were considered across the Mach-number range, with the Mach 25 conditions taken to 90 degrees angle of attack and the Mach 27.5 cases taken to 60 degrees angle of attack. Detailed surface heat-transfer rates were computed at Mach 20 and 25, revealing that heating rates on the heat-shield shoulder can exceed the stagnation-point heating by 230 percent. Finite-rate chemistry solutions were performed above Mach 10, otherwise perfect gas computations were made. Drag, lift, and pitching moment coefficients are computed and details of a wake flow are presented. The effect of including the wake in the solution domain was investigated and base pressure corrections to forebody drag coefficients were numerically determined for the lower Mach numbers. Pitching moment comparisons are made with direct simulation Monte Carlo results in the more rarefied flow at the highest Mach numbers, showing agreement within two-percent. Thin-layer Navier-Stokes computations of the axial force are found to be 15 percent higher across the speed range than the empirical/Newtonian based results used during the initial trajectory analyses.

Nomenclature

C_D	Drag coefficient
C_L	Lift coefficient
C_m	Pitching moment coefficient
M	Mach number
q	Heat transfer rate, W/cm^2
T	Temperature, K
V	Velocity, m/s
X, Y, Z	Cartesian coordinates
α	Angle of attack, degrees
γ	Ratio of specific heats
ρ	density, kg/m^3

Subscript:

∞	freestream value

Introduction

The Commercial Experiment Transporter[1,2] (COMET) is a new space enterprise to place small payloads in a micro-gravity environment for 30 days and return them to Earth. COMET, managed by EER Systems Corp., grew out of NASA's Centers for the Commercial Development of Space program.[3] A low-cost approach toward development of the COMET return system was undertaken by relying heavily upon engineering analysis tools rather than state-of-the-art computational fluid dynamic techniques and ground-based testing. Prior to EER assuming control of the whole project in 1994, Space Industries, Inc. determined preliminary aerodynamic coefficients during the design phase from empirical correlations or modified Newtonian calculations.[4] Contracts[5] have been set for a first launch during the autumn of 1995* from Wallops Island, Va., with splash-down in the Atlantic Ocean off the Virginia

*Aerospace Technologist, Aerothermodynamics Branch, Gas Dynamics Division. Member AIAA.
†Aerospace Technologist, Aerothermodynamics Branch, Gas Dynamics Division. AIAA Associate Fellow.
‡Aerospace Technologist, Aerothermodynamics Branch, Gas Dynamics Division.

*Destroyed in launch explosion, October 23, 1995.

coast. The first launch is not a demonstration flight, but rather a fully-operational mission with payloads. The operational vehicle is to be named METEOR–Multiple Experiment Transporter to Earth Orbit and Return.

Since COMET is launched and recovered from a NASA facility, NASA undertook a mission safety assessment of the reentry capsule to ensure minimal risk to population centers, performing additional trajectory and landing-footprint analyses. The NASA trajectories sought to refine the dispersion analyses[6] used during program development to a state-of-the-art level. While liability in the commercial space sector[7] is becoming a strong driver for mission successes, the NASA program focused primarily on mission safety issues, trying for conservative estimates on landing dispersions. Close communication and cross-feedback with EER was maintained throughout the NASA project. This effort provided input to the Department of Transportation review conducted as part of licensing the return system.

In support of these trajectory analyses the present study provided an improved aerodynamic dataset for the COMET reentry capsule throughout the hypersonic and supersonic flight regimes. Three-sigma uncertainties on aerodynamics used in previous dispersion analyses were estimated at 10–20 percent.[8] The current study applies Euler and Navier-Stokes class algorithms, including reacting flow gas chemistry, to obtain more comprehensive predictions for the lift, drag, and moment coefficients, used to refine the dispersion analysis of the COMET reentry capsule.

Configuration

The COMET reentry capsule, pictured in profile in Fig. 1, is an axisymmetric design with a spherical heat-shield of 48-in. radius. The frontal diameter and area are 52 in. and 2124 in.^{2}, respectively, and are the nondimensionalizing length and area used in computing the aerodynamic coefficients. All moment coefficients reported here are referenced to a point on the axis of revolution 17.6 in. back from the nosetip. The heat-shield is composed of a moderate-density, filled silicone syntactic foam in a phenolic-fiberglass honeycomb. An approximation to the true vehicle geometry was made on the base, which is modeled here as a flat disc connecting the sides with the rocket nozzle cover. In reality this region is recessed by approximately four inches and the volume occupied by the parachutes.

Algorithm

The Langley Aerothermodynamic Upwind Relaxation Algorithm (LAURA)[9–11] was used to generate the computational aerodynamic predictions in the current

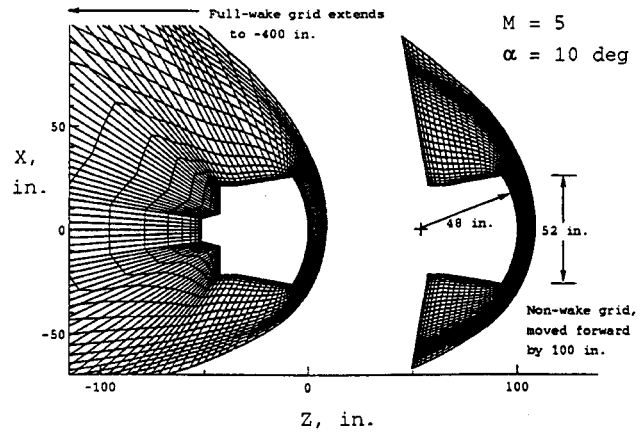

Fig. 1 Sample full-flowfield and non-wake symmetry plane grids, coarsened to show every-other body-normal point.

study. LAURA is an upwind, point-implicit, second-order-accurate fluid dynamics solver based on an extension of the Roe flux-difference-splitting scheme[12] that has been used to analyze such reentry capsules as the Aeroassist Flight Experiment[13] and Mars Pathfinder Mission.[14]

Both Euler and laminar thin-layer Navier-Stokes solutions were obtained with LAURA about the COMET vehicle with perfect-gas ($\gamma = 1.4$) and seven-species, one- and two-temperature, finite-rate air. A fully-catalytic wall boundary condition was employed for the reacting cases. Steady-state assumptions were imposed. A plane of symmetry was assumed for three-dimensional solutions and circumferential symmetry was assumed for axisymmetric solutions. The vehicle rotation, nominally three revolutions per minute at the atmospheric entry point, was not modeled.

Modifications were made to LAURA during this study to facilitate grid adaptions with wake flows by terminating the downstream grid 350 inches from the body, approximately seven vehicle diameters. Also, an entropy condition check was installed for defining the bow shock location in the grid alignment procedure to handle low-Mach-number wakes. An energy limiter was applied as necessary during the initial transitory solution time to prevent non-physical conditions from developing on the vehicle base.

Computational Grid

The computational grid used 64 cells in the body-normal direction, 36 cells circumferentially for the three-dimensional cases, and 66–72 cells down the body for the full-wake solutions. A close-up view of a full-wake-grid symmetry plane can be seen in the left-half of Fig. 1.

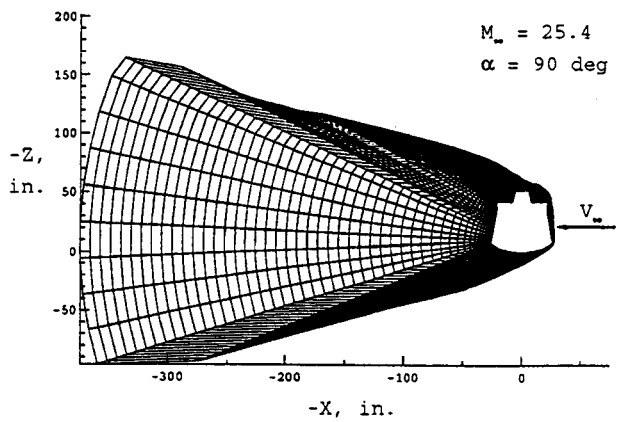

Fig. 2 High-angle-of-attack full-flowfield grid.

Calculations in the wake region assumed a laminar shear layer.

Grids without wakes, seen on the right side of Fig. 1, encompassed the forebody heat-shield and vehicle sidewalls, back to the 90 degree corner where the base begins, 43 inches from the nose. This breakpoint was chosen for the non-wake solutions because the flow typically undergoes a strong expansion at that point, limiting the upstream influence of the wake on the forebody flowfield.

The grids were initially generated algebraically and then adapted as the solution evolved, aligning the grid with the bow shock and clustering points in the boundary layer. A full wake grid is presented in Fig. 2 for a Mach 25, 90 degree angle-of-attack case, highlighting the wake flow grid-adaption results.

For the aerodynamic calculations the heat-shield shoulder is modeled as a sharp corner. Due to extremely high heating the corner is anticipated to ablate into a naturally rounded shoulder. To investigate the surface heating distribution more realistically in the vicinity of the heat-shield shoulder, three solutions about the peak heating portion of the trajectory, at Mach 20 and 25, were obtained with a quarter-inch (0.635 cm) shoulder radius. Eight computational cells were used to define the shoulder in these cases, with a total of 95 streamwise cells used to ease the grid stretching around the shoulder. Although the shoulder rounding is expected to occur in flight due to ablation, no ablative effects were modeled in the computations. An ablative and/or finite-catalycity heat-shield would be expected to lower the heating rates, so the heat-transfer computations here are conservative predictions. The effect of a shoulder radius did not influence the vehicle aerodynamics.

Grid convergence was spot checked with respect to convergence of the vehicle aerodynamic coefficients. At Mach 25 and 30 degrees angle of attack the viscous, seven-species, two-temperature solution was obtained on $48 \times 12 \times 64$, $95 \times 18 \times 64$, and $95 \times 36 \times 64$-cell grids, counting streamwise, circumferentially, and normal to the body. The 64 points in the body-normal direction were chosen based on the grid convergence analysis performed by Weilmuenster[15] Axial force coefficients are within one percent on all three grids and pitching moment coefficients, compared to the finest-grid results, are within three percent on the coarsest grid and one percent on the intermediate grid.

Cases

An initial trajectory was defined by the POST[16] code based on the preliminary engineering approximations to the COMET aerodynamics. The capsule is expected to enter the rarefied atmosphere at approximately 70 degrees angle of attack. While deceleration and heating loads are low in the free molecular and transitional domains, the accurate determination of the pitching moment at these altitudes is essential to determine if the capsule will weather-cock into a heat-shield-first attitude by the time it reaches the continuum atmosphere, defined as Knudson numbers less than order 1, or below 90 km for the COMET vehicle. A concurrent study computed a matrix of flowfield simulations in the transitional domain between the free molecular and continuum limits using a direct simulation Monte Carlo (DSMC) approach.

The DSMC code was originally devised by Bird[17] and extended for applications to complex geometries by Rault.[18] This approach tracks a large ensemble of discrete molecules, handling all the physics through molecular collisions rather than with fluid equations of motion. DSMC is currently the only practical technique with sufficient accuracy to realistically simulate very rarefied kinetics. Results of this DSMC study indicated that the COMET reentry capsule will generate enough turning moment to rotate the vehicle to a heat-shield-first attitude by 90 km altitude. A sampling of the DSMC results are presented here showing continuity of pitching moment determinations between DSMC and LAURA.

Thirty-six complete computational fluid dynamics solutions were obtained with LAURA at discrete Mach numbers ranging from 1.5–27 and an angle-of-attack range of 0–20 degrees. Side-slip was not modeled, as the vehicle is axisymmetric. The Mach 20, 25, and 27 cases were taken to 30, 90, and 60 degrees, respectively. The freestream conditions for each trajectory point are enumerated in Table 1, as well as a specification to whether the solutions were viscous or inviscid, with perfect gas or reacting air chemistry, and with or without the base-wake domain included in the calculations.

Table 1 COMET trajectory points.

M_∞	V_∞, m/s	ρ_∞, kg/m^3	T_∞, K	α, deg
1.51	451	3.84×10^{-2}	212	0^b; 5^a; 10^b; 20^b
2.00	601	2.68×10^{-2}	224	0^b; 5^a; 10^b; 20^a
5.06	1560	8.88×10^{-3}	236	0^b; 5^a; 10^b; 20^a
9.97	3200	3.12×10^{-3}	255	0^b; 5^a; 10^a; 20^a
15.1	5006	1.14×10^{-3}	271	0^c; 5^c; 10^c; 20^c
20.1	6429	4.31×10^{-4}	255	0^c; 5^c; 10^c; 15^d; 20^c; 30^d
25.4	7442	5.84×10^{-5}	213	0^d; 5^d; 10^c; 20^d; 30^d; 40^d; 60^d; 90^d
27.5	7563	3.41×10^{-6}	187	0^d; 20^d; 40^d; 60^d

[a]Perfect gas, inviscid.
[b]Perfect gas, viscous, wake included.
[c]Reacting air, viscous.
[d]Reacting air, viscous, wake included.

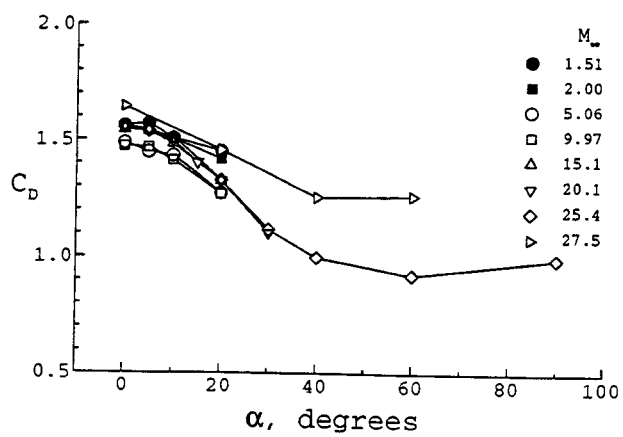

Fig. 3 COMET drag coefficients.

Table 2 COMET aerodynamic coefficients.

M_∞		Angle of attack, deg. 0	5	10	20
1.51	C_D	1.56	1.57	1.51	1.45
	C_L	0.	-0.0586	-0.208	-0.266
	C_m	0.	-0.0256	-0.0429	-0.0809
2.00	C_D	1.55	1.54	1.50	1.42
	C_L	0.	-0.0734	-0.170	-0.233
	C_m	0.	-0.0210	-0.0374	-0.0755
5.06	C_D	1.49	1.45	1.43	1.27
	C_L	0.	-0.0882	-0.172	-0.280
	C_m	0.	-0.0152	-0.0302	-0.0591
9.97	C_D	1.47	1.47	1.41	1.27
	C_L	0.	-0.0912	-0.171	-0.291
	C_m	0.	-0.0151	-0.0301	-0.0575
15.1	C_D	1.54	1.54	1.48	1.32
	C_L	0.	-0.0929	-0.179	-0.312
	C_m	0.	-0.0169	-0.0326	-0.0594
20.1	C_D	1.56	1.54	1.49	1.32
	C_L	0.	-0.0981	-0.188	-0.320
	C_m	0.	-0.0165	-0.0323	-0.0597
25.4	C_D	1.55	1.54	1.51	1.33
	C_L	0.	-0.0962	-0.187	-0.310
	C_m	0.	-0.0167	-0.0318	-0.0602
27.5	C_D	1.64	–	–	1.45
	C_L	0.	–	–	-0.262
	C_m	0.	–	–	-0.0554

Results

Aerodynamic coefficients

Drag, lift, and moment coefficients, respectively, are plotted in Figs. 3–5 versus angle of attack for the eight trajectory points. The aerodynamic data is tabulated in Table 2, for 0–20 degrees angle of attack, Table 3, for 40–90 degrees angle of attack, and Table 4, for the three heating cases.

The COMET vehicle is at a maximum-drag condition, Fig. 3, about zero angle of attack. The zero-angle-of-attack drag coefficients vary between 1.55 at Mach 1.5 and 2, down below 1.5 as the Mach number increases to 10, then rise back to 1.55 by Mach 25 and above as the freestream conditions become more rarefied. Comparing drag coefficients with the more approximate methods used in Ref. 4 show that the current results predict a 15 percent higher drag for COMET. The correspondingly lower ballistic coefficient indicates more deceleration at higher altitudes and reduces the down-range flight distance of the reentry capsule relative to the preliminary design analyses.

Negative lift is generated by the free-flying capsule, seen in Fig. 4. This behavior is expected with the very blunt configuration producing an axial force that dominates the normal force. The lift-curve slope is relatively constant between 0–20 degrees angle of attack at -0.015 per degree. The largest magnitude lift-to-drag ratio is -0.32 for Mach 20, 30 degree angle-of-attack conditions. At the higher Mach numbers the vehicle is seen to return to a zero-lift condition at 60 degrees angle of attack. The 90 degree angle-of-attack solution also has

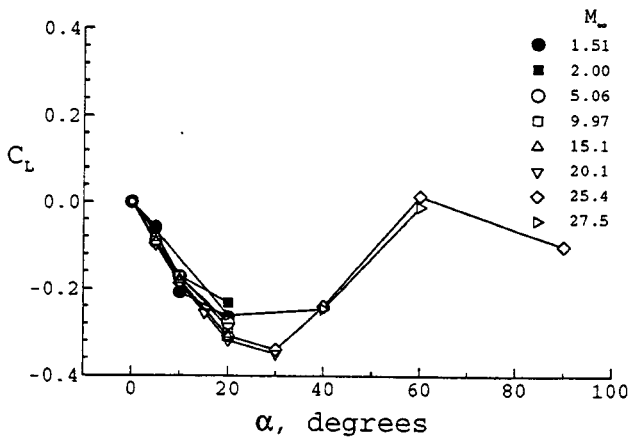

Fig. 4 COMET lift coefficients.

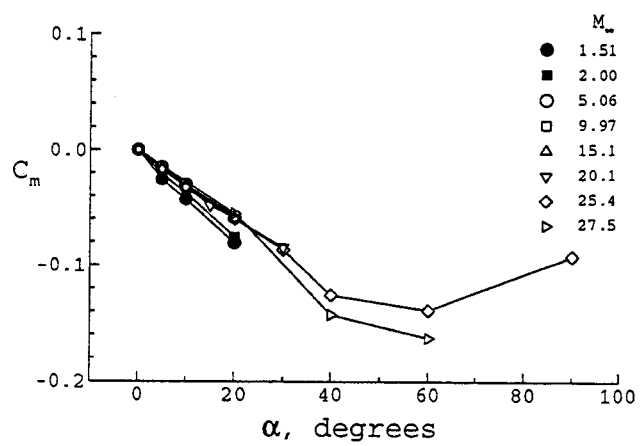

Fig. 5 COMET moment coefficients.

Table 3 COMET high-angle-of-attack aerodynamic coefficients.

		Angle of attack, deg.		
M_∞		40	60	90
25.4	C_D	0.997	0.923	0.994
	C_L	-0.240	0.0137	-0.102
	C_m	-0.126	-0.139	-0.0923
27.5	C_D	1.25	1.26	–
	C_L	-0.247	-0.0117	–
	C_m	-0.143	-0.163	–

Table 4 Aerodynamics and heating about peak heating trajectory point.

		Angle of attack, deg.	
M_∞		15	30
20.1	C_D	1.40	1.101
	C_L	-0.256	-0.3509
	C_m	-0.04837	-0.08494
	q_{stag}	77.5 W/cm^2	90.7 W/cm^2
	$q_{shoulder}$	129. W/cm^2	200. W/cm^2
25.4	C_D	–	1.116
	C_L	–	-0.3413
	C_m	–	-0.08684
	q_{stag}	–	60.1 W/cm^2
	$q_{shoulder}$	–	138. W/cm^2

negative lift, though the data is too sparse in the 40–90 degree angle-of-attack range to accurately define the lift trends there.

COMET is statically stable, Fig. 5, with a negative pitching moment across the angle-of-attack range, trimmed at zero angle of attack. The moment coefficient slope has an average value of -0.0032 per degree between 0–40 degrees angle of attack, nearly independent of Mach number. Beyond 60 degrees angle of attack the vehicle becomes less stable, though the moment is still negative so a restoring moment toward zero angle of attack is maintained.

The variation in pitching-moment coefficient with altitude at 60 degrees angle of attack is presented in Fig. 6. The altitudes range from the rarefied regime above 135 km, where the free-molecular calculation is appropriate, through the transitional freestream conditions computed with the DSMC code, to the continuum results of LAURA. Very good agreement is seen between LAURA and DSMC at the overlap point at 90 km, where the DSMC moment coefficient differs by two percent from the LAURA prediction. The results of a modified Newtonian calculation are included at the continuum altitudes for comparison, and are seen to differ by 12 percent from the LAURA solution at 75 km altitude.

Wake effects

Base pressure corrections were made to the axial force coefficient for three of the cases. This was to correct for neglecting the wake region in these solutions. For the Mach 1.5, 5 degree angle-of-attack case the axial force coefficient was increased by 18 percent. At Mach 2 the axial force coefficients for both 5 and 20 degree angles-of-attack were increased by 11 percent. These corrections were obtained from the 0 and 10 degree angle-of-attack cases done at Mach 1.5 and 2, which were computed both with and without the wake. At Mach 5 the difference between axial force coefficients for solutions with

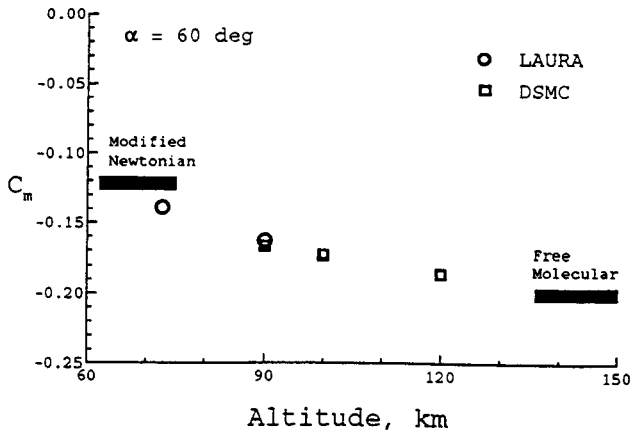

Fig. 6 Pitching moment coefficients at high altitudes.

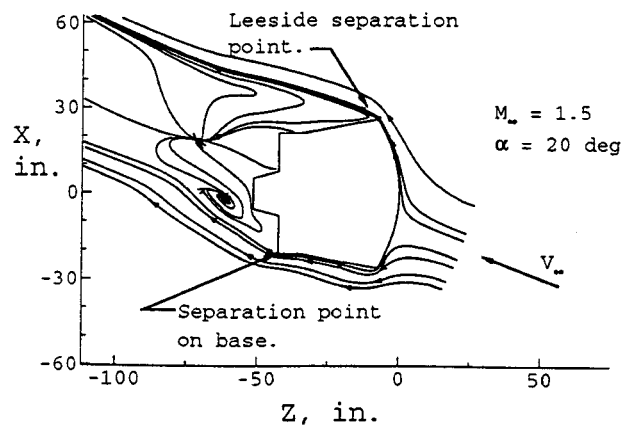

Fig. 7 Streamlines detailing wake recirculation region at Mach 1.5.

and without wake computations was 0.02, or 1.3 percent. Above Mach 5 the difference between aerodynamic coefficients from solutions with and without wakes was negligible for small angles-of-attack. Base pressure corrections were not made to the solutions which neglected the wake at Mach 5 and above. All solutions at angles of attack above 20 degrees included the wake domain.

Comparing the computed base-pressure corrections with those from a common engineering formula,[19]

$$\Delta C_{D,\ base\ correction} = \frac{1}{M_\infty^2} - \frac{0.57}{M_\infty^4}$$

show this expression yields corrections 24 percent larger than those from the LAURA study at Mach 1.5.

At small angles of attack over most of the trajectory the wake recirculation region is confined to the base of the vehicle and a forebody flowfield solution plus base-pressure correction obtains accurate vehicle aerodynamics. At the lower Mach numbers, particularly Mach 1.5, and moderate angles of attack the wake recirculation is not confined to the base of the vehicle, making the base-pressure correction approach less reliable.

Figure 7 shows a close-up view of the streamlines in the symmetry plane around the vehicle and in the wake for Mach 1.5, 20 degree angle-of-attack conditions. The laminar thin-layer approximation was used in all calculations. The flowfield can be seen to separate on the leeside at the heat-shield shoulder. A large recirculation region in the wake extends from the base up and around the entire leeside of the vehicle. A three-dimensional structure in the wake can be seen in the source and sink toroidal vortex behind the vehicle. Fluid is entrained at the windside center of the vortex, located approximately 10 in. behind the retro-rocket nozzle. The fluid is pumped around the toroid and emerges in the symmetry plane as a source located at coordinates $(-75, 20)$ in Fig. 7.

Effect of gas model and viscosity

Calculations with both perfect-gas and finite-rate chemistry were made at Mach 5 and 10 axisymmetric conditions. At Mach 5 the reacting-flow drag coefficient is 0.6 percent higher than the perfect-gas result. At Mach 10 the reacting-flow drag is computed to be two percent higher than perfect-gas drag, as 1.516. Finite-rate calculations were made for all cases above Mach 10.

Comparisons were also made between viscous and inviscid perfect gas calculations for the axisymmetric, Mach 5 conditions. The inviscid drag coefficient, 1.462, is within 0.3 percent of the viscous result, 1.458, with both solutions performed without the wake domain. This is because the post-shock pressure on the heat-shield is the dominant contributer to drag, and no separation at the shoulder was seen at the lower angles of attack. The perfect-gas, non-wake results presented here were inviscid calculations, and all wake-inclusive and reacting-flow solutions were viscous calculations.

Heating

Surface heat-transfer rates were computed about the expected peak heating time of the reentry trajectory. Results at Mach 20 with 15 and 30 degrees angle of attack and Mach 25 at 30 degrees angle of attack are presented in Table 4 for the stagnation point and maximum shoulder heating. While the manufactured capsule has a sharp corner at the edge of the heat-shield, in-flight degradation during reentry is expected to naturally round the shoulder. For the results presented here the shoulder radius was *a priori* set to 0.25 in. (6.4 mm).

The small shoulder radius causes a strong expansion and acceleration of the flow around the edge of the heat-shield, thinning the boundary layer considerably

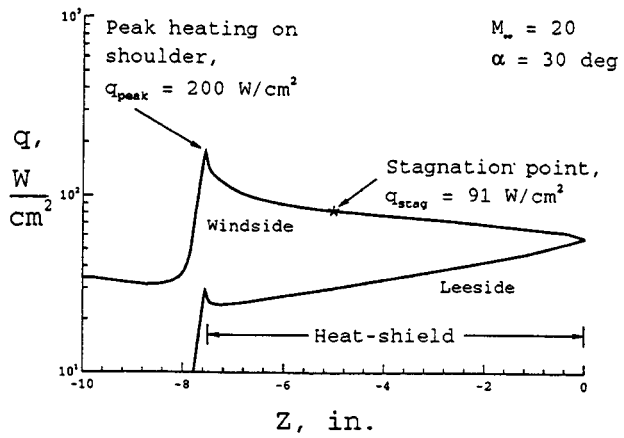

Fig. 8 Centerline heat-transfer rates over forebody heat-shield.

and producing locally high heating on the shoulder. The degree of this heating spike is seen to depend upon angle of attack, as for the 15 degree angle-of-attack case the peak heating is 1.7 times the stagnation-point heating while for the two 30 degree angle-of-attack cases the peak heating on the shoulder is 2.2–2.3 times the stagnation-point heating, reaching a maximum of 200 W/cm^2 at Mach 20.

Windside and leeside centerline surface heat-transfer rates for the Mach 20, 30 degree angle-of-attack conditions are displayed in Fig. 8. This plot zooms in on the heat-shield and shoulder region, extending along the axial axis 8 in. (20 cm) back from the nose-tip. For this case, Fig. 8 does not show a heat-transfer peak along the centerline at the stagnation point, as might be expected on the spherical heat-shield. The stagnation point itself was located as the maximum in the surface pressure data. Significant spikes in the heating are seen at the heat-shield shoulder on both the wind and lee sides. While the high shoulder-heating rates on the windside are of concern for determining the heat-shield thickness, the vehicle rotation during reentry will tend to distribute the shoulder heat load around the circumference of the heat-shield.

Summary of Results

An aerothermodynamic analysis of the Commercial Experiment Transporter (COMET) reentry capsule has been performed using the Langley Aerothermodynamic Upwind Relaxation Algorithm. Steady-state laminar thin-layer Navier-Stokes and Euler flowfield solutions were obtained at eight trajectory points for Mach numbers 1.5, 2.0, 5.1, 10.0, 15.1, 20.1, 25.4, and 27.5. Axisymmetric and 5, 10, and 20 degree angles of attack were considered across the Mach-number range, with the Mach 25.4 conditions taken to 90 degrees angle of attack and the Mach 27.5 cases taken to 60 degrees angle of attack. Perfect gas computations were performed for the Mach 10 and lower cases, while finite-rate-chemistry air calculations were made for Mach numbers above 10. Comparison calculations at Mach 10 showed a two percent difference in drag coefficient between perfect-gas and finite-rate solutions, with even less difference seen at Mach 5, as would be expected.

Two solution domains were solved: one full-vehicle grid encompassing the wake region and a second grid encompassing the heat-shield and sidewall domains, but not the base or wake. The wake was neglected on the low angle of attack solutions between Mach 10 and 20. A base pressure correction was made to the axial force coefficient at Mach 1.5, 5 degrees angle of attack and Mach 2, 5 and 20 degree angles of attack. These base pressure corrections were determined from repeated calculations at Mach 1.5 and 2 using grids both with and without the wake domain. The effect of including the wake on vehicle aerodynamics was found to be negligible at higher Mach numbers. All high-angle-of-attack cases included the wake domain.

Surface heat-transfer rates were computed at Mach 20 and 25, with particular attention paid to the heat-shield shoulder region. Peak shoulder heating can be 2.2–2.3 times the stagnation point heat-transfer rate, computed assuming no ablation and a fully-catalytic wall.

Axisymmetric drag coefficients varied from a low of 1.47 at Mach 10 to a high of 1.64 at Mach 27.5. The drag coefficient decreases at non-zero angles of attack. Negative lift is generated at angles of incidence, with the lift coefficient varying between 0 and -0.32. The vehicle is statically stable, trimmed about zero angle of attack, with a value of approximately -0.0032 per degree for $C_{m,\alpha}$ between 0–40 degrees angle of attack.

These aerodynamic results differ by 15 percent from the previously published data, and are being used in refined landing-footprint analyses to ensure a safe splashdown location, and to position the recovery ship for swifter capsule retrieval.

References

[1]F. C. Wessling, M. Robinson, R. S. Martinez, T. Gallimore, and N. Combs, "Commercial Experiment Transporter—COMET," *Journal of Spacecraft and Rockets*, vol. 31, pp. 846–854, Septempber-October 1994.

[2]T. Ajluni and J. Hager, "Comet: Creating the United States' First Complete Commercial Space Service," AIAA Paper 92–1564, March 1992.

[3]B. A. Stone, "Space Commerce: Preparing for the Next Century," IAA Paper 91–643, October 1991.

[4]S. M. Hill and T. McCusker, "COMET Recovery System Flight Dynamics," AIAA Paper 93–3693, 1993.

[5]P. Seitz, "NASA Signs Comet Contract, July Launch Set," *Space News*, p. 6, April 3–April 9 1995.

[6]S. M. Hill, "Preliminary COMET Recovery System Targeting and Dispersions," AIAA Paper 92–4659, 1992.

[7]P. D. Bostwick, "Liability of Aerospace Manufacturers: *MacPherson v. Buick* Sputters into the Space Age," *Journal of Space Law*, vol. 22, no. 1–2, pp. 75–96, 1994.

[8]T. J. McCusker and S. M. Hill, "Landing Dispersions for the Commercial Experiment Transporter Recovery System," AIAA Paper 93–3695, 1993.

[9]P. A. Gnoffo, R. N. Gupta, and J. L. Shinn, "Conservation Equations and Physical Models for Hypersonic Air Flows in Thermal and Chemical Nonequilibrium," NASA TP 2867, February 1989.

[10]P. A. Gnoffo, "An Upwind-Biased, Point-Implicit Relaxation Algorithm for Viscous, Compressible Perfect-Gas Flows," NASA TP 2953, February 1990.

[11]P. A. Gnoffo, "Point-Implicit Relaxation Strategies for Viscous, Hypersonic Flows," in *Computational Methods in Hypersonic Aerodynamics* (T. K. S. Murthy, ed.), pp. 115–151, Kluwer Academic Publishers, 1991.

[12]P. L. Roe, "Approximate Riemann Solvers, Parameter Vectors, and Difference Schemes," *Journal of Computational Physics*, vol. 43, pp. 357–372, October 1981.

[13]P. A. Gnoffo, "Code Calibration Program in Support of the Aeroassist Flight Experiment," *Journal of Spacecraft and Rockets*, vol. 27, pp. 131–142, March-April 1990.

[14]R. A. Mitcheltree and P. A. Gnoffo, "Wake Flow about a MESUR Mars Entry Vehicle," AIAA Paper 94–1958, June 1994.

[15]K. J. Weilmuenster and P. A. Gnoffo, "Solution Strategy for Three-Dimensional Configurations at Hypersonic Speeds," *Journal of Spacecraft and Rockets*, vol. 30, pp. 385–394, July-August 1993.

[16]G. L. Brauer, D. E. Cornick, and R. Stevenson, "Capabilities and Applications of the Program to Optimize Simulated Trajectories (POST)," NASA CR 2770, Feb. 1977.

[17]G. A. Bird, *Molecular Gas Dynamics.* Oxford: Clarendon Press, 1976.

[18]D. F. G. Rault, "Aerodynamics of the Shuttle Orbiter at High Altitudes," *Journal of Spacecraft and Rockets*, vol. 31, pp. 944–952, Nov. 1994.

[19]E. Bonner, W. Clever, and K. Dunn, "Aerodynamic Preliminary Analysis System II. Part I—Theory," NASA CR 165627, 1989.